METROLOGY AND MEASUREMENT SYSTEMS
Index 330930, ISSN 0860-8229
www.metrology.pg.gda.pl

A DESIGN FRAMEWORK FOR RIGOROUS CONSTRAINED EM-DRIVEN OPTIMIZATION OF MINIATURIZED ANTENNAS WITH CIRCULAR POLARIZATION

Adrian Bekasiewicz[1)], Slawomir Koziel[1, 2)]

1) *Gdańsk University of Technology, Faculty of Electronics, Telecommunications and Informatics, G. Narutowicza 11/12, 80-233 Gdańsk, Poland* (✉ *bekasiewicz@ru.is*, +48 58 347 2019)
2) *Reykjavik University, Engineering Optimization & Modeling Center, School of Science and Engineering, 101 Reykjavik, Iceland* (*koziel@ru.is*)

Abstract

Compact radiators with circular polarization are important components of modern mobile communication systems. Their design is a challenging process which requires maintaining simultaneous control over several performance figures but also the structure size. In this work, a novel design framework for multi-stage constrained miniaturization of antennas with circular polarization is presented. The method involves sequential optimization of the radiator in respect of selected performance figures and, eventually, the size. Optimizations are performed with iteratively increased number of design constraints. Numerical efficiency of the method is ensured using a fast local-search algorithm embedded in a trust-region framework. The proposed design framework is demonstrated using a compact planar radiator with circular polarization. The optimized antenna is characterized by a small size of 271 mm^2 with 37% and 47% bandwidths in respect of 10 dB return loss and 3 dB axial ratio, respectively. The structure is benchmarked against the state-of-the-art circular polarization antennas. Numerical results are confirmed by measurements of the fabricated antenna prototype.

Keywords: axial ratio, antenna miniaturization, circular polarization antenna, constrained optimization, EM-driven design.

1. Introduction

Rapid development of mobile communication systems has been driving interest towards design of compact antennas featuring low *axial ratio* (AR) within a broad range of operating frequencies. *Circular polarization* (CP) antennas found applications in various systems including radio-frequency identification [1, 2], GPS [3, 4] but also wearable and Internet-of-Things devices [5–8] as well as rectifiers for RF energy harvesting [8, 9]. CP operation enables to maintain a connection between the transmitter and the receiver regardless their mutual orientation. Moreover, it is important for increasing the immunity of the communication system to the weather conditions and multipath fading [10]. Small size and large AR bandwidth belong to the most desired properties of modern CP antennas as they are important for mobility of the system, as well as simplification of its TX/RX path.

Article history: received on Oct. 02, 2018; accepted on Oct. 30, 2018; available online on Mar. 29, 2019, DOI: 10.24425/mms.2019.126331.

The most popular methods for exciting CP radiation in the antenna include the use of multiple feeding ports [11–13], and modifications of radiator topology [14–16]. In multi-port radiators, the AR level is typically controlled through a feeding network which provides an appropriate phase shift and power levels at the antenna inputs [11–13]. However, the use of multi-point feeds often increases geometrical complexity (also, by promoting multi-layer topologies [11–13]) which negatively affects the size of the antenna and increases its manufacturing costs. Furthermore, the structures with external feeding networks are characterized by a relatively narrow 3 dB AR bandwidth [3, 13]. Consequently, single-feed structures for which the CP behaviour is obtained as a result of unconventional topology of the radiator are preferable for space-limited applications. Such structures maintain low AR by exploiting various geometrical alterations such as adding stubs, slots and/or various parasitic components [15–17]. Compact CP structures can be also obtained using open-slot topologies with L-shaped [15], or T-shaped [16] slots. When a low profile of the structure is not of primary concern, small footprint can be achieved using non-conventional patch topologies, or dielectric resonators [18, 19].

Broad AR bandwidth is one of the most important features of compact CP antennas. It is, however, difficult to be obtained. In the literature, wideband CP behaviour is often achieved using heavily modified topologies with multiple perforations within the radiator and the ground plane [20–22]. The mentioned challenges imply that making appropriate choices in the course of topology development of a compact CP antenna is crucial for its performance. Although various methods for automated evolution of antenna topologies have been reported in the literature, they are applicable to rather simple problems such as minimization of structure in-band reflection [23, 24]. From this perspective, manual topology development driven by engineering insight is still necessary when small antenna dimensions are to be achieved along with improved field and/or electrical performance [21].

Although the basic working mechanism of each modern antenna – including the CP ones – is determined during development of its topology, refinement of structure performance through adjustments of parameters is indispensable for obtaining acceptable performance. In the literature, the antenna dimensions are predominantly tuned based on parametric studies involving manual inspection of the characteristics [14, 17, 25, 26]. This approach is laborious and, more importantly, unsuitable for ensuring control over more than one performance figure at a time. Consequently, interactive design approaches are normally focused on minimization of antenna in-band reflection with size reduction and wideband CP operation being merely by-products of the parametric studies. Another challenge is that manual design approaches are useful only for problems with up to a few variables whereas modern CP antennas are characterized by complex, multi-parameter geometries [14, 21]. The mentioned challenges can be addressed by means of numerical optimization algorithms which enable to maintain control over selected figures of interest through simultaneous and unsupervised adjustment of all relevant design variables [27, 28]. Moreover, the ability of handling multiple performance figures at a time makes optimization algorithms a preferable tool for adjusting antenna performance and/or reduction of its size [29].

In this paper, a novel methodology for rigorous EM-driven design of compact antennas with circular polarization that enable implicit handling of performance-related constraints has been proposed. The procedure involves multi-stage optimization involving a gradient-based algorithm embedded within a *trust-region* (TR) framework [28]. In each design stage, different objective functions are used so that explicit optimization of antenna matching, *axial ratio* (AR) and size are performed sequentially. To ensure feasibility of the optimized designs, performance-related constraints are defined for the last two steps. The proposed approach has been used for performance adjustment and miniaturization of a planar CP antenna. The optimized radiator is characterized by small dimensions of 16.2 mm × 16.7 mm with the overall footprint of only 271 mm^2. The minia-

turized structure features in-band reflection and AR of around −10 dB and 2.7 dB, respectively. The optimized antenna is compared with the state-of-the-art CP radiators. The simulation data are validated through measurements of the fabricated antenna prototype.

2. Compact antenna with circular polarization

Figure 1 shows geometry of the CP antenna considered for the sake of demonstrating the optimization framework proposed in this work. The structure is implemented on a 0.762-mm-thick Taconic RF-35 dielectric substrate ($\varepsilon_r = 3.5, \tan\delta = 0.0018$). It is a compact planar radiator with two elliptical slots and two symmetrical side notches within the ground plane. The antenna radiating element – in the form of a strip with two asymmetrical stubs connected to its opposite edges – enables, upon appropriate sizing, to excite orthogonal electric field vectors with equal amplitudes thus launching CP radiation. The radiator is fed through a 50 Ohm micro-strip line. Although the structure is based on a work of [14], it includes several modifications that enables to improve the control over its in-band axial ratio and reflection while ensuring compact dimensions. The topology changes include introduction of the low impedance load in the stub connected to the antenna feed, removal of notches within the circular slot (*cf.* Fig. 1), as well as re-parameterization of the geometry using relative variables. The latter is important for maintaining consistency of the structure at each design stage.

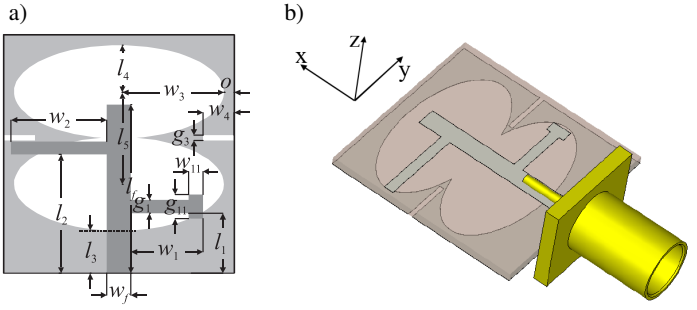

Fig. 1. A compact antenna structure with circular polarization: a) topology of the considered radiator with marked adjustable parameters (a dotted line denotes location of the edge of the lower elliptical slot); b) a 3D view of the structure with the SMA connector.

The antenna design is described by a fifteen-variable vector $\boldsymbol{x} = [l_{fr}\ l_{1r}\ l_{2r}\ l_3\ l_4\ l_5\ w_{1r}\ w_{11}\ w_{2r}\ w_3\ w_{4r}\ g_1\ g_{11}\ g_3\ o]^T$. The relative parameters are $l_f = (l_3 + 2l_5 + l_6 + o)l_{fr}$, $l_1 = (l_f - g_1)l_{1r}$, $l_2 = (l_f - g_2)l_{2r}$, $w_1 = 0.5(2w_3 + 2o - w_f)w_{1r}$, $w_2 = 0.5(2w_3 + 2o - w_f)w_{2r}$, and $w_4 = 0.5(2w_3 + 2o)w_{4r}$. The dimension $w_f = 1.7$ remains fixed to ensure 50 Ohm impedance at the antenna input. All dimensions, except the unit-less ones with the r in subscript, are in mm. The following lower and upper bounds: $\boldsymbol{l} = [0.5\ 0.1\ 0.5\ 2\ 2\ 4\ 0.5\ 0.2\ 0.5\ 5\ 0.2\ 0.2\ 0.2\ 0.2\ 0.2]^T$ and $\boldsymbol{u} = [1\ 0.6\ 1\ 5\ 5\ 8\ 1\ 3\ 1\ 8\ 0.7\ 1.2\ 2.0\ 1.2\ 3]^T$ are defined to maintain consistency of the radiator in the course of its optimization. The operational bandwidth of the antenna is from 5 GHz to 7 GHz, which makes it suitable for certain C-band applications such as 5.2 GHz and 5.8 GHz wireless LAN, as well as industrial, scientific, and medical radio.

The *electromagnetic* (EM) model $\boldsymbol{R}$ of the antenna is implemented in CST Microwave Studio and evaluated using its transient solver [30]. For reliability of EM simulation results – the considered structure is electrically small [31] – the model is supplemented with a SubMiniature

version A (SMA) connector (see Fig. 1b). The model is discretized using approximately 1,600,000 mesh cells and its average evaluation time on a dual Xeon E5540 machine is 10 min.

3. Design methodology

In this section, a methodology for efficient EM-driven constrained optimization of CP antennas is presented. Specifically, we formulate the design optimization problem and discuss the employed trust-region-based optimization algorithm. Finally, we describe in detail the proposed design framework. Numerical results are provided in Section 4.

3.1. Problem formulation

The antenna design problem can be formulated as the following nonlinear minimization task:

$$\boldsymbol{x}^* = \arg\min_{x} U(\boldsymbol{R}(\boldsymbol{x})), \tag{1}$$

where $\boldsymbol{R}$ is the EM antenna model, U is a scalar objective function evaluated for a given vector of adjustable parameters $\boldsymbol{x}$, and $\boldsymbol{x}^*$ is the optimum design to be found. Here, the following design requirements are considered:

- Minimization of the antenna footprint;
- Maintaining the antenna reflection within the band of interest below −10 dB;
- Maintaining the in-band axial ratio below 3 dB.

It should be noted that evaluation of the constraints imposed on the AR and matching is expensive as it involves EM simulation of the antenna model. Appropriate handling of the constraints has been one of the incentives for development of an efficient optimization framework as described in the following sections.

3.2. Optimization algorithm

Due to a high cost of antenna model evaluation, direct solving of (1) within an EM-driven optimization setup is expensive, and, in many cases, impractical. Here, the problem is handled using a gradient-based algorithm embedded in the *trust-region* (TR) framework [28]. More specifically, we replace direct optimization of the EM model $\boldsymbol{R}$ by an iterative process that yields a series of approximations $\boldsymbol{x}^{(i)}$, $i = 0, 1, \ldots$, to $\boldsymbol{x}^*$ by solving:

$$\boldsymbol{x}^{(i+1)} = \arg\min_{\boldsymbol{x}:\ \|\boldsymbol{x}-\boldsymbol{x}^{(i)}\| \le \delta^{(i)}} U(\boldsymbol{G}^{(i)}(\boldsymbol{x})). \tag{2}$$

Here, $\boldsymbol{G}^{(i)}$ is the first-order Taylor expansion model of the form:

$$\boldsymbol{G}^{(i)}(\boldsymbol{x}) = \boldsymbol{R}(\boldsymbol{x}^{(i)}) + \boldsymbol{J}(\boldsymbol{x}^{(i)})(\boldsymbol{x} - \boldsymbol{x}^{(i)}). \tag{3}$$

A Jacobian $\boldsymbol{J}$ of the model response $\boldsymbol{R}$ is obtained using finite differentiation as:

$$\boldsymbol{J}(\boldsymbol{x}^{(i)}) = \left[\frac{\boldsymbol{R}(\boldsymbol{x}^{(i)} + \boldsymbol{h}_1) - \boldsymbol{R}(\boldsymbol{x}^{(i)})}{h_1} \quad \cdots \quad \frac{\boldsymbol{R}(\boldsymbol{x}^{(i)} + \boldsymbol{h}_N) - \boldsymbol{R}(\boldsymbol{x}^{(i)})}{h_N} \right]^T, \tag{4}$$

where $\boldsymbol{h} = [h_1 \ \ldots \ h_k \ \ldots \ h_N]^T$, $k = 1, \ldots, N$ (N is the number of adjustable design parameters), is a vector of perturbations around $\boldsymbol{x}^{(i)}$ and $\boldsymbol{h}_k = [0 \ \ldots \ h_k \ \ldots \ 0]^T$. The trust region radius $\delta^{(i)}$

is updated using the standard rules based on the gain ratio ρ which measures the actual versus predicted improvement of the objective function U [28]:

$$\rho = \frac{U(\boldsymbol{R}(\boldsymbol{x}^{(i+1)})) - U(\boldsymbol{R}(\boldsymbol{x}^{(i)}))}{U(\boldsymbol{G}^{(i)}(\boldsymbol{x}^{(i+1)})) - U(\boldsymbol{G}^{(i)}(\boldsymbol{x}^{(i)}))} . \tag{5}$$

At the beginning of the optimization process, the radius is $\delta^{(0)} = 1$. It is updated as follows. If the gain ratio $\rho > 0.75$ then the radius is set to $\delta^{(i+1)} = 2 \cdot \delta^{(i)}$, whereas if $\rho < 0.25$, it is set to $\delta^{(i+1)} = \delta^{(i)}/3$. The algorithm (2) is terminated when either $\delta^{(i)}$ or the distance between the designs obtained in two consecutive iterations is below 10^{-3}.

It should be noted that the considered TR-based algorithm is numerically efficient. Its computational cost is $N + 1$ evaluations of the EM antenna model per successful iteration ($\rho \geq 0$). Each unsuccessful iteration ($\rho < 0$) involves an additional EM simulation. For more information about the considered TR-based routine, see [28, 32].

3.3. Antenna design framework

The proposed design optimization framework consists of three stages, each involving the algorithm of Subsection 3.2. In the first step, the antenna is optimized to minimize in-band reflection. Subsequently, optimization oriented towards minimization of AR while maintaining a required matching level is considered. Finally, explicit reduction of the antenna size is carried out with constraints imposed on both axial ratio and reflection.

Due to the use of linear expansion models, explicit constraint handling in (2) is inconvenient. This is because approximation of the constraints provided by the model (3), may lead to an infeasible starting point for the subsequent algorithm iteration. Here, the problem is addressed by implicit constraint handling using a penalty function approach [29]. It should be noted that sequential introduction of constraints is important for maintaining performance figures at acceptable levels at the beginning of each design stage. Considering all objectives and constraints from the very beginning of the optimization process normally leads to inferior results due to high nonlinearity of the functional landscape imposed by the penalty functions (see below).

The objectives of the design process are formulated below. Let $S(\boldsymbol{x})$ and $AR(\boldsymbol{x})$ be the maximum reflection and the maximum axial ratio within the frequency range of interest, whereas $A(\boldsymbol{x})$ be the antenna footprint. In the first design stage, minimization of the antenna in-band reflection is performed by minimizing the following objective function:

$$U_1(\boldsymbol{R}(\boldsymbol{x})) = S(\boldsymbol{x}). \tag{6}$$

The optimized design $\boldsymbol{x}_1^*$ is then used as a starting point for solving a constrained problem given by:

$$U_2(\boldsymbol{R}(\boldsymbol{x})) = AR(\boldsymbol{x}) + \beta_2 c_2(\boldsymbol{x})^2. \tag{7}$$

Here, the term $c_2(\boldsymbol{x})$ is a penalty function of the form:

$$c_2(\boldsymbol{x}) = \max\left\{\frac{S(\boldsymbol{x}) + 10}{10},\ 0\right\}, \tag{8}$$

which measures a relative violation of the requirement concerning maximum acceptable in-band reflection (here, -10 dB). The coefficient β_2 is used to control the contribution of the penalty function to the overall objective. In other words, it permits adjusting the user "tolerance" for

violating the constraint. Here, we use $\beta_2 = 10$ which ensures a noticeable contribution for $S(\boldsymbol{x}) + 10$ exceeding a fraction of dB.

The design $\boldsymbol{x}_2^*$ obtained by minimizing (7) is used as a starting point for the third design stage. The objective function for constrained explicit size reduction is defined as:

$$U_3(\boldsymbol{R}(\boldsymbol{x})) = A(\boldsymbol{x}) + \beta_{3.1} c_2(\boldsymbol{x})^2 + \beta_{3.2} c_3(\boldsymbol{x})^2. \tag{9}$$

The penalty function $c_3(\boldsymbol{x})$, which enables implicit control of AR-related constraint, is defined as:

$$c_3(\boldsymbol{x}) = \max\left\{\frac{AR(\boldsymbol{x}) - 3}{3},\ 0\right\}. \tag{10}$$

The penalty coefficients in (9) are set to $\beta_{3.1} = 1000$ and $\beta_{3.2} = 100$ to ensure a noticeable contribution of (8) and (10) to the objective function for relatively low violation of the constraints. Note that the value of the coefficient controlling c_2 has been increased by two orders of magnitude, which is because typical values of $A(\boldsymbol{x})$ are a few hundred of mm^2 as opposed to a few dB for $AR(\boldsymbol{x})$.

The proposed multi-stage optimization algorithm can be summarized as follows:

1. Set $k = 1$ and an initial design $\boldsymbol{x}_k^{(0)} = \boldsymbol{x}_0$;
2. Set $U(\boldsymbol{R}(\boldsymbol{x})) = U_k(\boldsymbol{R}(\boldsymbol{x}))$ and find $\boldsymbol{x}_k^*$ starting from $\boldsymbol{x}_k^{(0)}$ using the algorithm of Subsection 3.2;
3. If $k = 3$, $\boldsymbol{x}^* = \boldsymbol{x}_k^*$ and END; Otherwise, set $k = k + 1$ and go to 2.

It should be noted that the implicit constraint handling considered here may lead to slight violation of constraints at the optimized designs [29, 32]. While increasing the penalty factors could prevent this effect, it would make the optimization problem more challenging due to increasing nonlinearity of the objective function in the vicinity of the feasible region boundary. Consequently, exploration of this boundary would be more difficult (especially due to numerical noise inherent to EM simulation data). It is of primary importance as the constraints are normally active at the optimum designs (*i.e.*, the designs are located at the feasible region boundary [33]).

4. Results and discussion

Here, the methodology introduced in Section 3 is demonstrated using the antenna structure considered in Section 2. Specifically, we focus on analysis of the numerical results, as well as comparison of the optimized antenna with the reference structure of [14] as well as the benchmark radiators. Finally, we discuss results of the experimental validation of the fabricated antenna prototype.

4.1. Numerical results

The antenna structure of Fig. 1 has been optimized using the methodology of Section 3. The initial design for the optimization process $\boldsymbol{x}_0 = [0.85\ 0.42\ 0.84\ 3\ 3.6\ 6.5\ 0.75\ 1\ 0.95\ 7.5\ 0.48\ 0.85\ 1.7\ 0.4\ 1]^T$ has been obtained through semi-manual modifications of the re-scaled dimensions of the reference radiator [14]. The design $\boldsymbol{x}_1^* = [0.71\ 0.39\ 0.86\ 3.1\ 3.47\ 6.63\ 0.68\ 1\ 0.94\ 7.62\ 0.38\ 0.92\ 1.67\ 0.38\ 1.05]^T$ was found by optimizing (6) after 9 iterations of the TR algorithm. The maximum reflection level for the optimized structure is −13.8 dB, whereas its maximum AR level is 3.2 dB, both within 5 GHz to 7 GHz band of interest. It should be noted that optimization of the antenna w.r.t. reduced reflection resulted in worsening of the AR compared with $\boldsymbol{x}_0$ (*cf.* Fig. 2).

However, it also resulted in improvement of in-band reflection by over 10 dB. The dimensions of the optimized design are 17.4 mm × 17.8 mm with the footprint of 308 mm^2.

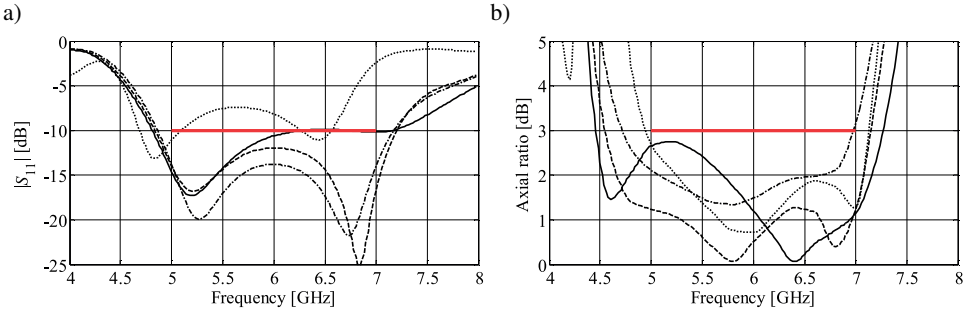

Fig. 2. Performance characteristics of the considered antenna with circular polarization obtained for the design $\boldsymbol{x}_0$ ($\cdots$), $\boldsymbol{x}_1^*$ ($-\cdot-$), $\boldsymbol{x}_2^*$ ($--$), and $\boldsymbol{x}_3^*$ (—): a) reflection, and b) axial ratio.

In the next step, the design $\boldsymbol{x}_1^*$ has been used as a starting point for explicit minimization of AR with constraint on $S(\boldsymbol{x})$. The final design $\boldsymbol{x}_2^*$ = [0.72 0.39 0.76 3.09 3.48 6.57 0.68 1 0.92 7.6 0.26 0.93 1.68 0.36 1.05]^T was obtained after 12 iterations of the algorithm of Section 2. The optimized antenna features the maximum in-band reflection of −12 dB and AR of only 1.3 dB. It maintains the reflection below the −10 dB level from 4.84 GHz to 7.2 GHz (2.36 GHz or 40% in respect of the centre frequency f_0 = 5 GHz). At the same time, its 3 dB AR bandwidth is from 4.54 GHz to 7.15 GHz (2.61 GHz). The external dimensions of the optimized structure are 17.3 mm × 17.7 mm with the footprint of 306 mm^2, which (despite lack of explicit size control) is slightly smaller than the footprint of design $\boldsymbol{x}_1^*$.

Finally, explicit size reduction of the antenna with constrains imposed on both performance requirements was performed using (9). The optimal design $\boldsymbol{x}^* = \boldsymbol{x}_3^*$ = [0.71 0.38 0.76 2.99 3.27 6.45 0.69 1 0.93 7.38 0.27 0.93 1.69 0.36 0.72]^T was obtained after 15 iterations of the algorithm (2). The size of the optimized antenna is 271 mm^2 (dimensions: 16.2 mm × 16.7 mm) which is over 11% smaller compared with $\boldsymbol{x}_2^*$. The structure features the maximum in-band reflection and AR of −9.8 dB and 2.75 dB, respectively. At the same time, its 3 dB AR is from 4.46 GHz to 7.28 GHz (2.82 GHz or 47%). It should be noted that only the constraint imposed on electrical performance is active in the final design. The reason is that antenna dimensions directly affect the length of the free space wave for which antenna can be coupled to [31]. Consequently,

Table 1. Compact CP antenna: comparison with Benchmark structures.

Design	f_L **[GHz]**	f_0 **[GHz]**	**AR BW [%]**	$\lvert S_{11}\rvert$ **BW [%]**	**Dimensions [mm × mm]**	**Size [mm^2]**	**Size [λ_g^2]**
[9]	2.40	2.44	2.05	5.73	60.0 × 60.0	3600	0.77
[34]	4.20	4.95	20.2	30.3	34.5 × 28.0	1190	0.63
[35]	1.82	2.45	56.7	51.4	70.0 × 70.0	4900	0.64
[26]	4.73	5.65	36.1	46.3	20.0 × 17.8	356	0.25
[14] (Fig. 3)	4.60	5.80	45.2	41.4	20.4 × 19.0	388	0.26
[14]	4.41	6.15	36.9	57.2	20.0 × 20.0	400	0.29
This work	4.82	6.00	47.0	36.7	16.2 × 16.7	271	0.19

miniaturized antennas often feature close-to-threshold electrical performance. At the same time, the AR-related performance can be maintained at an acceptable level through modifications of the radiator geometry which, in case of the considered antenna, does not have a direct effect on the size. A comparison of antenna reflection and AR responses at the $\boldsymbol{x}_0$ and at each step of the design process is shown in Fig. 2.

The computational cost of the design optimization process is 381 simulations of the EM antenna model (~ 64 hours) and it includes 114, 117, and 150 evaluations of the RF model for the first, second, and third stage of the design process of Subsection 3.3. It should be noted that gradual increase of the number of evaluations required to complete each design step results from growing complexity of the design problem caused by sequential introduction of performance constraints.

4.2. Discussion and comparisons

To evaluate the effects of geometrical changes discussed in Section 2 on size reduction of the considered antenna, the methodology of Section 3 has also been used to design the reference structure of [14]. The comparison of performance characteristics obtained for both radiators is shown in Fig. 3. The results indicate that despite a larger complexity and a larger number of adjustable dimensions (17 instead of 15) the structure of [14] is characterized by a narrower 3 dB AR bandwidth than the antenna considered here (2.62 GHz versus 2.84 GHz, respectively). At the same time, bandwidths of both structures are the same (2.4 GHz). However, the −10 dB corner frequency of the reference structure is shifted down by 200 MHz compared with the modified radiator (4.6 GHz vs. 4.8 GHz). More importantly, the size of antenna of [14] is over 30% larger compared with the size of the modified structure (388 mm^2 vs. 271 mm^2).

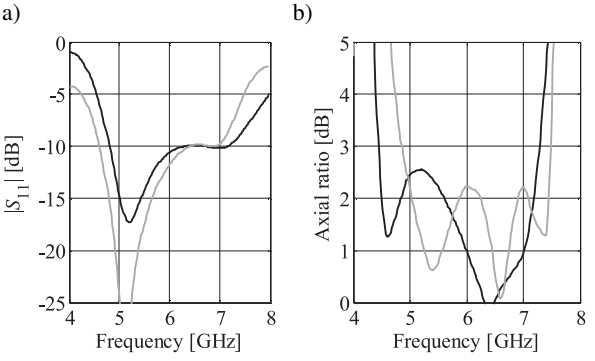

Fig. 3. Comparison of frequency characteristics of the modified antenna (black) and the reference structure of [14] (grey) obtained using the methodology of Section 3: a) reflection, and b) axial ratio.

The optimized radiator of Section 2 has also been compared with the state-of-the-art structures with CP polarization in terms of size, as well as bandwidth defined in respect of 3 dB AR and −10 dB reflection levels [9, 14, 26, 34, 35]. In order to account for differences between various substrate materials, dimensions of the benchmark structures are expressed in terms of the guided wavelength λ_g (calculated for the lower corner frequency f_L of the −10 dB reflection band and the given electrical parameters of the substrate). Also, due to the differences between the antenna centre frequencies (f_0), AR and reflection bandwidths are expressed in relative terms.

The obtained results indicate that the considered antenna structure features the smallest size, while providing competitive AR and reflection bandwidths. Although the antenna of [35] offers better performance compared with the considered one, this is achieved at a cost of over three times larger size (wavelength-wise). It should be noted that, despite re-optimization (*cf.* Fig. 3), the antenna of [14] features a narrower AR BW and a larger size which confirms that the introduced topological modifications are important for reducing the radiator size while maintaining its acceptable performance.

4.3. Experimental validation

The optimized radiator has been manufactured and measured. Fig. 4 shows a photograph of the fabricated antenna prototype. Comparison of the simulated Fig. 5, whereas the *xy*-plane RHCP

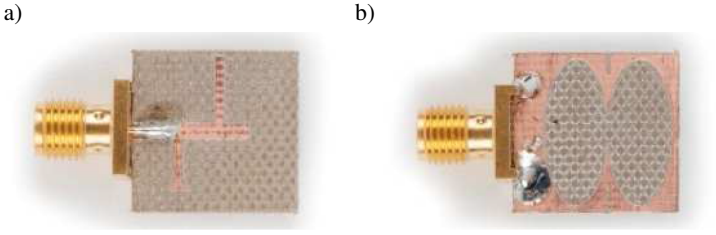

Fig. 4. A photograph of the considered antenna optimized for minimum size: a) front; b) back.

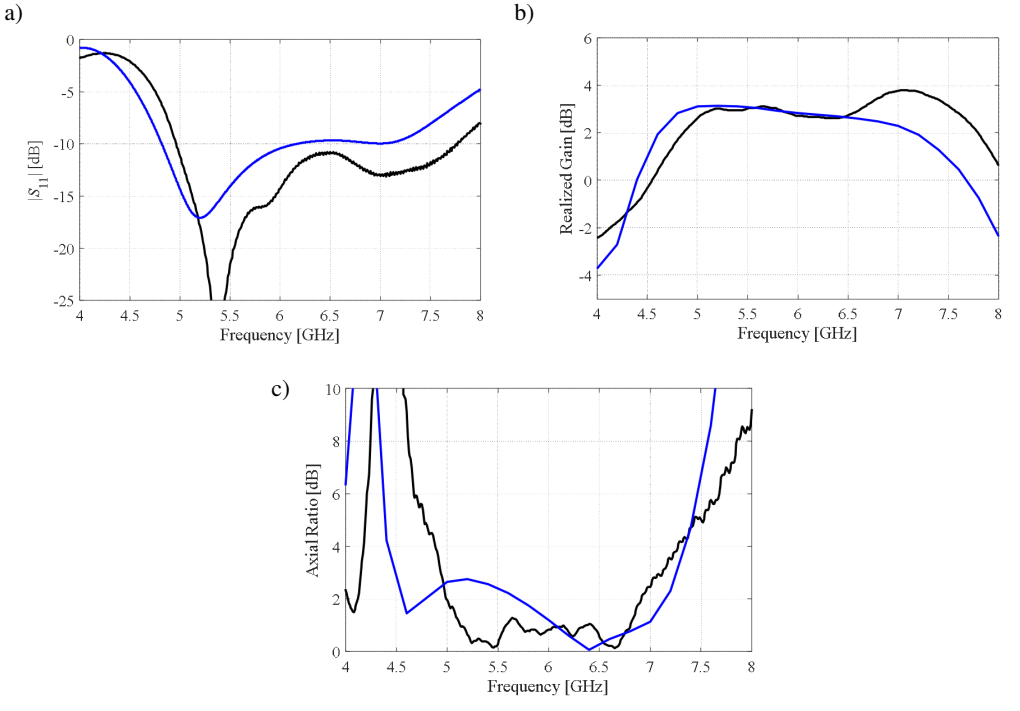

Fig. 5. Comparison of the simulated (blue) and measured (black) responses of the and measured reflection, axial ratio, and gain characteristics is shown in optimized antenna in terms of: a) reflection; b) realized gain; c) axial ratio.

and LHCP patterns for 5 GHz, 6 GHz, and 7 GHz, are shown in Fig. 6. The agreement between simulations and measurements is acceptable. The measured −10 dB impedance bandwidth is from 4.9 GHz to 7.8 GHz, whereas the measured 3 dB AR bandwidth is from 4.8 GHz to 7.2 GHz. The discrepancies between the simulated and measured responses are mostly a result of fabrication and assembly tolerances, as well as electrically large measurement setup, not taken into account in the antenna EM model. It should be noted that vertical discrepancies between the simulated and measured gain and AR characteristics are also affected by measurement tolerances within the anechoic chamber.

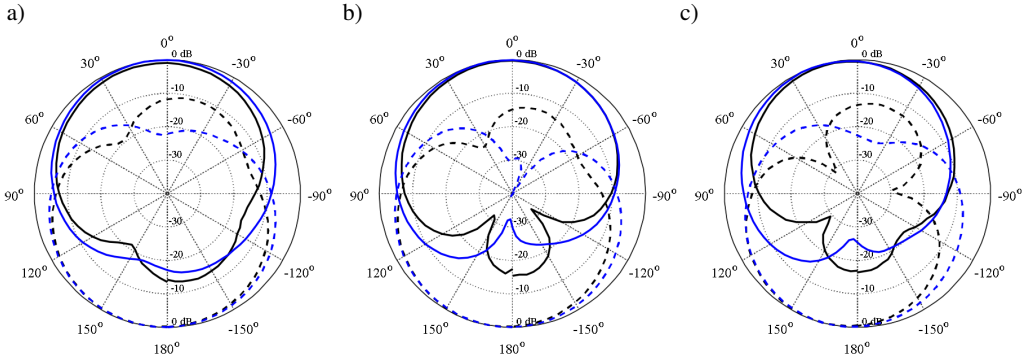

Fig. 6. Comparison of the simulated (blue) and measured (black) xy-plane right- (—) and left-handed CP (– –) radiation patterns obtained at: a) 5 GHz, b) 6 GHz, and c) 7 GHz.

5. Conclusion

A design framework for rigorous multi-stage constrained size reduction of CP antennas has been proposed. A low cost of the design process is maintained by using a numerically efficient local optimization algorithm embedded in a trust-region framework. The proposed design procedure has been demonstrated using a planar compact antenna with circular polarization which has been initially optimized for reduction of the in-band reflection, then optimized (with a reflection constraint) for minimum axial ratio and, finally, optimized for size reduction (with the AR and reflection constraints). The miniaturized structure is characterized by a footprint of only 271 mm^2 while ensuring 47% and 36.7% AR and reflection bandwidths (both in respect of 6 GHz centre frequency), respectively. The structure has been experimentally validated and favourably compared with the benchmark antennas reported in the literature. Our future work will focus on application of the proposed methodology to determination of extreme optimal designs prior to optimization of microwave/antenna structures in a multi-objective setup.

Acknowledgement

The authors would like to thank Computer Simulation Technology GmbH, a Dassault Systèmes Company, Darmstadt, Germany, for making CST Microwave Studio available. This work was supported in part by the Icelandic Centre for Research (RANNIS) Grant 174114051, and by National Science Centre of Poland Grant 2015/17/B/ST6/01857.

References

[1] Lu, J.H., Chang, B.S. (2017). Planar compact square-ring tag antenna with circular polarization for UHF RFID applications. *IEEE Trans. Ant. Prop.*, 65(2), 432–441.

[2] Pan, T., Zhang, S., He, S. (2014). Compact RFID tag antenna with circular polarization and embedded feed network for metallic objects. *IEEE Ant. Wireless Prop. Lett.*, 13, 1271–1274.

[3] Son, W.I., Lim, W.G., Lee, M.Q., Min, S.B., Yu, J.W. (2010). Design of compact quadruple inverted-F antenna with circular polarization for GPS receiver. *IEEE Trans. Ant. Prop.*, 58(5), 1503–1510.

[4] Wang, M.S., Zhu, X.Q., Guo, Y.X., Wu, W. (2018). Miniaturized dual-band circularly polarized quadruple inverted-F antenna for GPS applications. *IEEE Ant. Wireless Prop. Lett.*, 17(6), 1109–1113.

[5] Qu, L., Piao, H., Qu, Y., Kim, H.H., Kim, H. (2018). Circularly polarised MIMO ground radiation antennas for wearable devices. *Electronics Lett.*, 54(4), 189–190.

[6] Cheng, W., Li, D. (2017). Circularly polarised filtering monopole antenna based on miniaturised coupled filter. *Electronics Lett.*, 53(11), 700–702.

[7] Zahran, S.R., Hu, Z., Abdalla, M.A. (2017). A flexible circular polarized wide band slot antenna for indoor IoT applications. *IEEE Int. Symp. Ant. Prop.*, 1163–1164.

[8] Cao, Y., Hong, W., Deng, L., Li, S., Yin, L. (2016). A 2.4 GHz circular polarization rectenna with harmonic suppression for microwave power transmission. *IEEE Int. Conf. IoT*, 359–363.

[9] Huang, F.J., Yo, T.C., Lee, C.M., Luo, C.H. (2012). Design of circular polarization antenna with harmonic suppression for rectenna application. *IEEE Ant. Wireless Prop. Lett.*, 11, 592–595.

[10] Mener, S., Gillard, R., Roy, L. (2017). A dual-band dual-circular-polarization antenna for Ka-band satellite communications. *IEEE Ant. Wireless Prop. Lett.*, 16, 274–277.

[11] Han, J.H., Myung, N.H. (2014). Novel feed network for circular polarization antenna diversity. *IEEE Ant. Wireless Prop. Lett.*, 13, 979–982.

[12] Lin, W., Wong, H. (2017). Wideband circular-polarization reconfigurable antenna with L-Shaped feeding probes. *IEEE Ant. Wireless Prop. Lett.*, 16, 2114–2117.

[13] Ogurtsov, S., Koziel, S. (2016). Automated design of circularly polarized microstrip patch antennas with improved axial ratio. *Loughborough Ant. Prop. Conf.*, 1–5.

[14] Mohammadi, S., Nourinia, J., Ghobadi, C., Pourahmadazar, J., Shokri, M. (2013). Compact broadband circularly polarized slot antenna using two linked elliptical slots for C-band applications. *IEEE Ant. Wireless Prop. Lett.*, 12, 1094–1097.

[15] Wong, K.L., Huang, C.C., Chen, W.S. (2002). Printed ring slot antenna for circular polarization. *IEEE Trans. Ant. Prop.*, 50(1), 75–77.

[16] Wang, C.J., Shih, M.H., Chen, L.T. (2015). A wideband open-slot antenna with dual-band circular polarization. *IEEE Ant. Wireless Prop. Lett.*, 14, 1306–1309.

[17] Kumar, A., Deegwal, J.K., Sharma, M.M. (2018). Design of multi-polarised quad-band planar antenna with parasitic multistubs for multiband wireless communication. *IET Microwaves, Ant. Prop.*, 12(5), 718–726.

[18] Kovitz, J.M., Rajagopalan, H., Rahmat-Samii, Y. (2016). Circularly polarised half E-shaped patch antenna: a compact and fabrication-friendly design. *IET Microwaves, Ant. Prop.*, 10(9), 932–938.

[19] Wang, K.X., Wong, H. (2015). A circularly polarized antenna by using rotated-stair dielectric resonator. *IEEE Ant. Wireless Prop. Lett.*, 14, 787–790.

[20] Tang, H., Wang, K., Wu, R., Yu, C. (2016). ompact broadband CP monopole antenna with tilted branch. *Electronics Lett.*, 52(21), 1739–1740.

[21] Zhang, X.Y., Jiao, Y.C., Zhang, Z., Li, B. (2018). Miniaturised CP aperture antenna with tri-mode operation for broadening bandwidth. *Electronics Lett.*, 54(3), 122–124.

[22] Sun, Y.X., Leung, K.W., Mao, J.F. (2018). Dualfunction dielectric resonator as antenna and phase-delay-line load: designs of compact circularly polarized/differential antennas. *IEEE Trans. Ant. Prop.*, 66(1), 414–419.

[23] Ghassemi, M., Bakr, M., Sangary, N. (2013). Antenna design exploiting adjoint sensitivity-based geometry evolution. *IET Microwaves Ant. Prop.*, 7(4), 268–276.

[24] Toivanen, J.I., Makinen, R.A.E., Rahola, J., Jarvenpa, S., Yla-Oijala, P. (2010). Gradient-based shape optimisation of ultra-wideband antennas parameterised using splines. *IET Microwaves, Ant. Prop.*, 4(9), 1406–1414.

[25] Zhou, W., Liu, J., Long, Y. (2017). A broadband and high-gain planar complementary yagi array antenna with circular polarization. *IEEE Trans. Ant. Prop.*, 65(3), 1446–1451.

[26] Ahdi Rezaeieh, S., Abbosh, A., Antoniades, M.A. (2013). Compact CPW-fed planar monopole antenna with wide circular polarization bandwidth. *IEEE Ant. Wireless Prop. Lett.*, 12, 1295–1298.

[27] Nocedal, J., Wright, S. (2006). *Numerical Optimization*. 2nd edition, Springer, New York.

[28] Conn, A., Gould, N.I.M., Toint, P.L. (2000). *Trust-region methods*. MPS-SIAM Series on Optimization, Philadelphia.

[29] Koziel, S., Bekasiewicz, A. (2016). *Multi-objective design of antennas using surrogate models*. World Scientific.

[30] CST Microwave Studio, ver. 2013, CST AG, Bad Nauheimer Str. 19, D-64289 Darmstadt, Germany, 2013.

[31] Volakis, J., Chen, C.C., Fujimoto, K. (2010). *Small Antennas: Miniaturization Techniques and Applications.* McGraw-Hill Professiona.

[32] Koziel, S., Bekasiewicz, A. (2017). Expedited simulation-driven design optimization of UWB antennas by means of response features. *Int. J. RF Microwave CAE*, 27(6), 1–8.

[33] Johanesson, D.O., Koziel, S., Bekasiewicz, A. (2017). An improved procedure for simulation-driven miniaturization of antenna structures. *IEEE International Symposium on Antennas and Propagation*, San Diego.

[34] Wu, Z., Li, L., Li, Y., Chen, X. (2016). Metasurface superstrate antenna with wideband circular polarization for satellite communication application. *IEEE Ant. Wireless Prop. Lett.*, 15, 374–377.

[35] Fujimoto, T., Jono, K. (2014). Wideband rectangular printed monopole antenna for circular polarisation, *IET Microwaves, Ant. Prop.*, 8(9), 649–656.